

Out-of-equilibrium dynamics of Bose-Bose mixtures in optical latticesPardeep Kaur,¹ Kuldeep Suthar^{2,3}, Dilip Angom⁴, and Sandeep Gautam¹¹*Department of Physics, Indian Institute of Technology Ropar, Rupnagar 140001, Punjab, India*²*Institute of Atomic and Molecular Sciences, Academia Sinica, Taipei 10617, Taiwan*³*Department of Physics, Central University of Rajasthan, Ajmer 305817, Rajasthan, India*⁴*Department of Physics, Manipur University, Canchipur 795003, Manipur, India*

(Received 14 August 2023; accepted 12 December 2023; published 8 January 2024)

We examine the quench dynamics across quantum phase transitions from a Mott insulator (MI) to a superfluid (SF) phase in a two-component bosonic mixture in an optical lattice. We show that two-component Bose mixtures exhibit qualitatively different quantum dynamics than one-component Bose gas. In addition to second-order MI-SF transitions, we investigate quench dynamics across a first-order MI-SF phase boundary. The Bose mixtures show the critical slowing down of dynamics near the critical transition point, as proposed by the Kibble-Zurek mechanism. For MI-SF transitions with homogeneous lattice-site distributions in the MI phase, the dynamical critical exponents extracted by the power-law scaling of the proposed quantities obtained via numerical simulations are in very close agreement with the mean-field predictions.

DOI: [10.1103/PhysRevA.109.013308](https://doi.org/10.1103/PhysRevA.109.013308)**I. INTRODUCTION**

Ultracold atoms in quantum gas experiments provide an ideal platform to explore exotic quantum phases with unprecedented control over many-body dynamics [1,2]. These atoms confined within an optical lattice create a strongly correlated quantum system [3,4] with tunable parameters like interparticle interactions, lattice geometry, particle statistics, lattice depth, filling factors, and so on. The minimal model that describes the ground-state properties of bosonic atoms in an optical lattice is the Bose-Hubbard model (BHM) [3,5]. The BHM is crucial for exploring the quantum phase transitions [6] and the feasibility of quantum computing with cold atoms in optical lattices [7].

Studying out-of-equilibrium dynamics in interacting quantum systems and searching for an adiabatic state for quantum computation is an active research area [8]. Various methods can take a quantum system out of equilibrium, such as connecting it to an external bath, applying a driving field, or modifying one of the parameters in the underlying Hamiltonian during a quantum quench. The Kibble-Zurek [9,10] mechanism (KZM) offers a comprehensive theoretical framework to understand the nonequilibrium dynamics of such systems and predicts a universal power-law scaling of excitations as a function of the quench rate, with an exponent directly related to the equilibrium critical exponents [9–12]. Initially proposed to explain the evolution of the early universe [9], the KZM has been experimentally explored in various classical and quantum phase transitions. Its application has been demonstrated in numerous systems such as cosmic microwave background [13], liquid helium [14], superconductors [15], and liquid crystals [16]. More recently, studies on the KZM have been extended to ultracold quantum gases [17–19], where theoretical [20–25] as well as experimental studies [18,26,27] till now have focused on the one component Bose-Hubbard model.

In the present work, we theoretically examine the quench dynamics of Mott insulator-superfluid (MI-SF) phase transitions in the two-component Bose-Hubbard model (TBHM). A two-component Bose mixture in an optical lattice is not just an extension of a one-component Bose gas in a lattice as the phases of multicomponent and spinor systems in such scenarios are considerably more intricate [28]. In the miscible domain with equal intraspecies interactions, both components of the binary mixture occupy the same lattice site in an even-integer Mott lobe and the superfluid phase, yielding homogeneous atomic occupancy distributions of the two components, whereas for the odd-integer Mott lobes, the atomic occupancy distributions are inhomogeneous. Due to stronger interspecies repulsion in the phase-separated domain, neither component can occupy the same lattice site in any phase. The inhomogeneity of the phases in the TBHM may lead to novel dynamics. Moreover, the MI-SF transition in the one-component BHM is continuous. In contrast, the TBHM exhibits a tricritical point, after which the MI-SF transition changes to a first-order transition [29]. Although the KZM predicts the breakdown of adiabaticity for continuous transitions, both experimental [30,31] and theoretical studies [23,24] also confirm the critical slowing down for the first-order phase transitions. Motivated by these studies, we explore the first- and second-order MI-SF transitions of the TBHM in the present work and discuss the effects of the inhomogeneity of phases and order of transitions on the impulse regime and scaling exponents.

This paper is organized as follows. In Sec. II, we introduce the TBHM and describe the mean-field approach to determine the equilibrium phase diagram for three different values of the interspecies interactions corresponding to the miscible-immiscible phase transition. The dynamical Gutzwiller equations and the KZM are presented in Sec. III. Section IV discusses the quantum quench dynamics across MI(2)-SF and MI(1)-SF transitions of the TBHM, where

the number in the parentheses represents the total average atomic occupancy. Finally, we summarize our findings in Sec. V.

II. TWO-COMPONENT BOSE-HUBBARD MODEL

We consider a Bose-Bose mixture of two spin states from the same hyperfine-spin manifold in a two-dimensional (2D) square optical lattice at zero temperature. The TBHM describes a mixture of two bosonic species with the following model Hamiltonian [32]:

$$\begin{aligned} \hat{H} = & - \sum_{p,q,\sigma} \left[(J_x^\sigma \hat{b}_{p+1,q}^{\dagger\sigma} \hat{b}_{p,q}^\sigma + \text{H.c.}) + (J_y^\sigma \hat{b}_{p,q+1}^{\dagger\sigma} \hat{b}_{p,q}^\sigma \right. \\ & \left. + \text{H.c.}) - \frac{U_{\sigma\sigma}}{2} \hat{n}_{p,q}^\sigma (\hat{n}_{p,q}^\sigma - 1) + \mu_\sigma \hat{n}_{p,q}^\sigma \right] \\ & + \sum_{p,q} U_{\uparrow\downarrow} \hat{n}_{p,q}^\uparrow \hat{n}_{p,q}^\downarrow, \end{aligned} \quad (1)$$

where (p, q) is the index of lattice sites with p and q as the indices along the x and y directions, respectively. The lattice coordinates are $x = pa$ and $y = qa$, where a is the lattice spacing. Here $\sigma = (\uparrow, \downarrow)$ is the spin-state index, J_x^σ (J_y^σ) is the nearest-neighbor hopping strength along the x (y) direction, $\hat{b}_{p,q}^{\dagger\sigma}$ ($\hat{b}_{p,q}^\sigma$) is the creation (annihilation) operator, $\hat{n}_{p,q}^\sigma$ is the number operator at the site (p, q) , $U_{\sigma\sigma}$ is the intraspecies interaction strength, $U_{\uparrow\downarrow}$ is the interspecies interaction strength between the two components, and μ_σ is the chemical potential of the σ spin component.

A. Static Gutzwiller mean-field theory

To examine the ground-state properties of the model Hamiltonian [Eq. (1)], we use the single-site Gutzwiller mean-field (SGMF) theory [33,34]. We decompose annihilation ($\hat{b}_{p,q}^\sigma$) and creation ($\hat{b}_{p,q}^{\dagger\sigma}$) operators into the mean-field and fluctuation parts as $\hat{b}_{p,q}^\sigma = \phi_{p,q}^\sigma + \delta\hat{b}_{p,q}^\sigma$ and $\hat{b}_{p,q}^{\dagger\sigma} = \phi_{p,q}^{\sigma*} + \delta\hat{b}_{p,q}^{\dagger\sigma}$, where $\phi_{p,q}^\sigma$ ($\phi_{p,q}^{\sigma*}$) is the superfluid order parameter. The above approximation decouples the Hamiltonian [Eq. (1)] in lattice sites, and the Hamiltonian can be written as the sum of single-site Hamiltonians. The local Hamiltonian at the (p, q) th site is

$$\begin{aligned} \hat{h}_{p,q} = & - \sum_{\sigma} \left[J_x^\sigma (\hat{b}_{p+1,q}^{\dagger\sigma} \phi_{p,q}^\sigma + \phi_{p+1,q}^{\sigma*} \hat{b}_{p,q}^\sigma) + \text{H.c.} \right. \\ & \left. + J_y^\sigma (\hat{b}_{p,q+1}^{\dagger\sigma} \phi_{p,q}^\sigma + \phi_{p,q+1}^{\sigma*} \hat{b}_{p,q}^\sigma) + \text{H.c.} \right. \\ & \left. - \frac{U_{\sigma\sigma}}{2} \hat{n}_{p,q}^\sigma (\hat{n}_{p,q}^\sigma - 1) + \mu_\sigma \hat{n}_{p,q}^\sigma \right] + U_{\uparrow\downarrow} \hat{n}_{p,q}^\uparrow \hat{n}_{p,q}^\downarrow. \end{aligned} \quad (2)$$

The total mean-field Hamiltonian of the system is $\hat{H} = \sum_{p,q} \hat{h}_{p,q}$. To obtain the ground state, we self-consistently diagonalize the Hamiltonian at each lattice site. The many-body Gutzwiller wave function for the ground state is [35]

$$|\Psi\rangle = \prod_{p,q} |\psi\rangle_{p,q} = \prod_{p,q} \sum_{n_\uparrow, n_\downarrow} c_{n_\uparrow, n_\downarrow}^{(p,q)} |n_\uparrow, n_\downarrow\rangle_{p,q}. \quad (3)$$

Here $|n_\uparrow\rangle$ and $|n_\downarrow\rangle$ are Fock states with $n_\sigma \in [0, N_b - 1]$, where N_b is the dimension of the Fock space. The c-

numbers $c_{n_\uparrow, n_\downarrow}^{(p,q)}$ are the complex coefficients that satisfy the normalization condition $\sum_{n_\uparrow, n_\downarrow} |c_{n_\uparrow, n_\downarrow}^{(p,q)}|^2 = 1$. The superfluid order parameters of the two components are

$$\phi_{p,q}^\uparrow = {}_{p,q}\langle \psi | \hat{b}_{p,q}^\uparrow | \psi \rangle_{p,q} = \sum_{n_\uparrow, n_\downarrow} \sqrt{n_\uparrow} c_{n_\uparrow-1, n_\downarrow}^{(p,q)*} c_{n_\uparrow, n_\downarrow}^{(p,q)}, \quad (4a)$$

$$\phi_{p,q}^\downarrow = {}_{p,q}\langle \psi | \hat{b}_{p,q}^\downarrow | \psi \rangle_{p,q} = \sum_{n_\uparrow, n_\downarrow} \sqrt{n_\downarrow} c_{n_\uparrow, n_\downarrow-1}^{(p,q)*} c_{n_\uparrow, n_\downarrow}^{(p,q)}. \quad (4b)$$

The atomic occupancies of the components at a lattice site (p, q) are the expectation of the number operators and are given by

$$\rho_{p,q}^\uparrow = {}_{p,q}\langle \psi | \hat{n}_{p,q}^\uparrow | \psi \rangle_{p,q} = \sum_{n_\uparrow, n_\downarrow} n_\uparrow |c_{n_\uparrow, n_\downarrow}^{(p,q)}|^2, \quad (5a)$$

$$\rho_{p,q}^\downarrow = {}_{p,q}\langle \psi | \hat{n}_{p,q}^\downarrow | \psi \rangle_{p,q} = \sum_{n_\uparrow, n_\downarrow} n_\downarrow |c_{n_\uparrow, n_\downarrow}^{(p,q)}|^2. \quad (5b)$$

Since the local Hamiltonian $\hat{h}_{p,q}$ depends on $\phi_{p,q}^\sigma$ and $\hat{n}_{p,q}^\sigma$, therefore, in our numerical computations the initial state is considered as a complex random distribution of the Gutzwiller coefficients across the lattice. We then solve for the ground state of each site by diagonalizing the corresponding single-site Hamiltonian. The ground state of the following lattice site is computed using the updated superfluid order parameters. This process is repeated until all the sites of a square lattice are covered. One such sweep is identified as an iteration, and we repeat the process for the next iteration. The iterations are repeated until the requisite convergence criteria are satisfied. Our study used 50 initial random configurations to compute the equilibrium phase diagrams. This is to ensure that the minimum energy state has been achieved. We consider a lattice size of 8×8 and $N_b = 6$ and checked that by increasing the system size or N_b the phase diagrams do not alter.

B. Equilibrium phase diagrams

In the present work, we consider equal hopping strengths in both directions, i.e., $J_x^\sigma = J_y^\sigma = J$, and identical chemical potentials $\mu_\sigma = \mu$ and intraspecies interactions $U_{\sigma\sigma} = U$. We scale all energies with respect to U . Following the phase-separation criterion of the two components, determined by the strength of the interspecies interaction, we investigate the two regimes: $U_{\uparrow\downarrow} < 1$ and $U_{\uparrow\downarrow} > 1$. We use the Gutzwiller mean-field approach to obtain the phase diagrams of the TBHM. The model exhibits two phases: MI and SF phases [36–39].

1. Interspecies interaction $U_{\uparrow\downarrow} < 1$

We first consider $U_{\uparrow\downarrow} = 0.5$ and 0.9 in the miscible regime of the TBHM. In the MI phase, $\phi_{p,q}^\sigma$ is zero but nonzero in the superfluid phase. We use this criterion to determine the phase boundary between MI and SF phases in the J - μ plane; Figs. 1(a) and 1(b) show the phase diagrams for $U_{\uparrow\downarrow} = 0.5$ and 0.9 , respectively.

At $U_{\uparrow\downarrow} = 0.5$, the MI-SF quantum phase transitions for both odd- and even-occupancy Mott lobes are second-order transitions. However, at $U_{\uparrow\downarrow} = 0.9$, the MI-SF transitions are not entirely second order. We find that the change in the order-of-transition, near the tip of the MI(2) lobe, occurs at $U_{\uparrow\downarrow} = 0.65$. For $U_{\uparrow\downarrow} = 0.9$, as shown in Fig. 1(b), the tri-

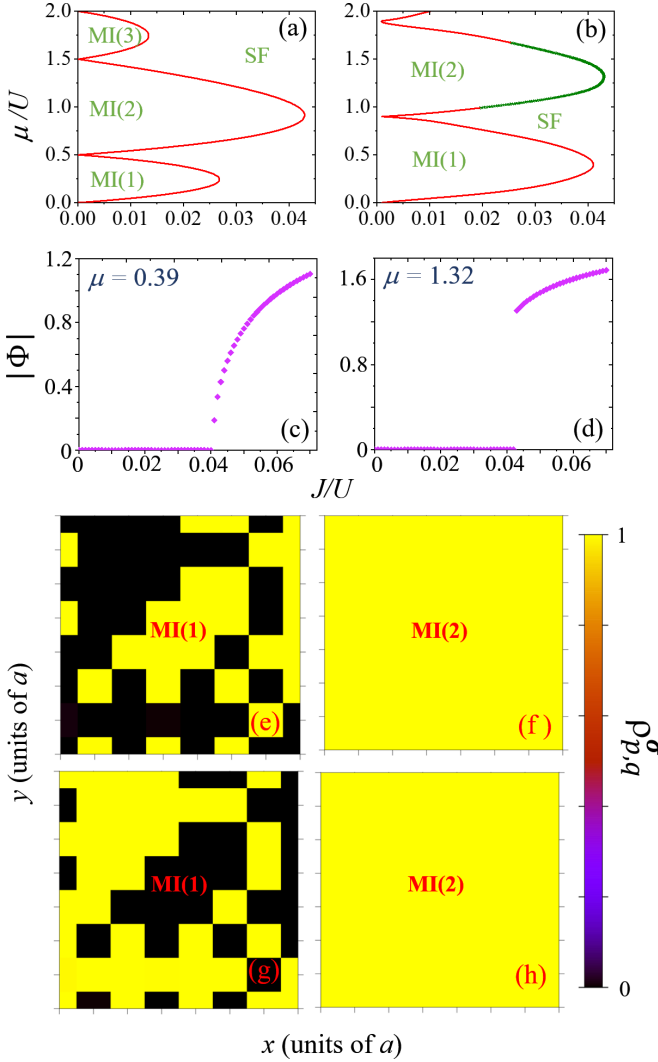


FIG. 1. Phase diagrams of the TBHM in J - μ plane for (a) $U_{\uparrow\downarrow} = 0.5$ and (b) $U_{\uparrow\downarrow} = 0.9$. The number in parentheses is the total average atomic occupancy $\sum_{\sigma} \rho^{\sigma}$, where for the MI(1) phase, the component average occupancies $\rho^{\sigma} = \sum_{p,q} \rho_{p,q}^{\sigma} / N_{\text{lattice}}$ are $0 < \rho^{\uparrow} < 1$, and $\rho^{\downarrow} = 1 - \rho^{\uparrow}$, and for the even-integer MI(2) phase, $\rho^{\uparrow} = \rho^{\downarrow} = 1$ [36]; here N_{lattice} is the number of lattice sites. In $J = 0$ limit, the size of the MI regions on the μ axis for odd and even total fillings are $U_{\uparrow\downarrow}$ and 1, respectively. The order of phase transition across all boundaries in (a) and (b) is second order except for the green curve in (b) across which the MI(2) to SF transition is of the first order. For $U_{\uparrow\downarrow} = 0.9$, the $|\Phi|$ as a function of J are shown for (c) MI(1)-SF transition at $\mu = 0.39$ and (d) MI(2)-SF transition at $\mu = 1.32$. In the third and fourth panels (e)–(h), sample atomic occupancy distributions ($\rho_{p,q}^{\sigma}$) on a 8×8 square lattice are shown. (e) and (g) correspond to $\rho_{p,q}^{\uparrow}$ and $\rho_{p,q}^{\downarrow}$, respectively, in the MI(1) phase. The same for MI(2) phase are shown in (f) and (h).

critical points on the μ axis exist at 0.99 and 1.67 between which the MI(2)-SF transition is of the first order [29,37,38]. To confirm the order of these transitions, we calculated the amplitude of the superfluid order parameter as a function of J for a fixed μ across the critical hopping strength. The continuous variation of $|\Phi| = \sum_{p,q,\sigma} |\phi_{p,q}^{\sigma}| / N_{\text{lattice}}$ with J represents a second-order phase transition as illustrated in Fig. 1(c) for

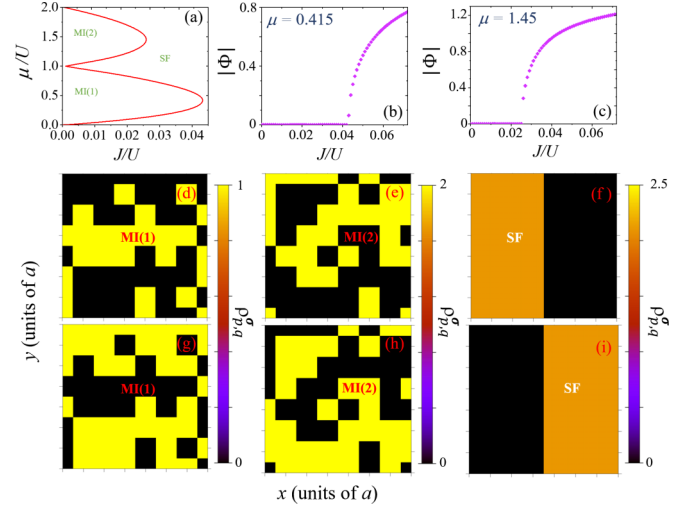


FIG. 2. (a) The phase diagram of the TBHM in J - μ plane in the immiscible regime. (b) The variation of $|\Phi|$ as a function of J with $\mu = 0.415$, corresponding to the MI(1)-SF phase transition and (c) with $\mu = 1.45$ corresponding to MI(2)-SF transition; these are plotted for $U_{\uparrow\downarrow} = 1.5$. The sample $\rho_{p,q}^{\uparrow}$ distributions in (d) MI(1), (e) MI(2), and (f) SF phases for $U_{\uparrow\downarrow} = 1.5$. Similarly, corresponding $\rho_{p,q}^{\downarrow}$ distributions are in (g), (h), and (i).

an MI(1)-SF phase transition with $\mu = 0.39$ and $U_{\uparrow\downarrow} = 0.9$. However, a discontinuity in $|\Phi|$ across the MI(2)-SF phase boundary in Fig. 1(d) for $\mu = 1.32$ and $U_{\uparrow\downarrow} = 0.9$ is indicative of the first-order phase transition. Using the perturbative mean-field theory in the SF domain near the MI($2m$)-SF phase boundary, where the SF order parameter is small with m as an integer, the single-site Ginzburg-Landau energy density function can be defined as $E(\phi) = \sum_{i=0,2,4,6} a_i \phi^i$. Here, the i th-order coefficient a_i can be expressed in terms of J , μ , U , $U_{\uparrow\downarrow}$, m , and $\phi = \phi_{\sigma}$ (order parameter) [29,38]. The transition across the MI($2m$)-SF phase boundary changes from second order to first order with a_4 changing from positive to negative with tricritical point(s) corresponding to $a_4 = 0$. It is to be noted that, in the single-component BHM, a_4 is always positive [40,41]. In addition, the study of the excitation spectrum across the MI(2)-SF phase boundary in the TBHM (using the Gutzwiller approximation) has shown that the excitation spectrum changes discontinuously across this first-order phase boundary [37]. Across the second-order SF-MI(2) phase transition, with a decrease in J/U , the low-energy parts of two gapped amplitude and two gapless sound modes merge at the phase boundary, whereas across the first-order transition, no gapped mode merges with the sound mode at the transition [37]. The sample atomic occupancy distributions $\rho_{p,q}^{\sigma}$ in MI(1) and MI(2) phases confined in $N_{\text{lattice}} = 8 \times 8$ square lattice are shown in Figs. 1(e), 1(g) and Figs. 1(f), 1(h), respectively. The atomic occupancy distributions in the SF phase are uniform and identical for both components with real occupancy.

2. Interspecies interaction $U_{\uparrow\downarrow} > 1$

For $U_{\uparrow\downarrow} > 1$, phase separation in the mixture occurs. We have shown the phase diagram for $U_{\uparrow\downarrow} = 1.5$ in Fig. 2(a), which does not change with an increase in $U_{\uparrow\downarrow}$. The continuous nature of the amplitude of the average superfluid order

parameter Φ as a function of J for $\mu = 0.415$ and 1.45 in Figs. 2(b) and 2(c), respectively, confirms the second-order nature of the MI-SF phase transitions. In this regime, only one of the components, chosen randomly, occupies the lattice site; the occupancy of the other component remains zero at that site. This applies to both the MI and SF phases. However, for the latter, the occupancy of one of the components is a real number and is zero for the other. The sample atomic occupancy distributions for MI(1), MI(2), and SF phases are presented in Figs. 2(d) and 2(g), Figs. 2(e) and 2(h), and Figs. 2(f) and 2(i), respectively.

III. QUENCH DYNAMICS

A. Time-dependent Gutzwiller approach

To study the out-of-equilibrium dynamics, we quench the hopping parameter in time, $J \rightarrow J(t)$, whereas all other model parameters remain fixed in time. The system will make the transition from the MI phase to the SF phase as J is ramped up in quench. The time-dependent Gutzwiller equation governs the time evolution of the single-site Gutzwiller wave function

$$i\hbar\partial_t|\psi\rangle_{p,q} = \hat{h}_{p,q}|\psi\rangle_{p,q}. \quad (6)$$

This leads to a system of coupled linear partial differential equations for the coefficients $c_{n_i, n_j}^{(p,q)}(t)$. To solve the coupled equations, we employ the fourth-order Runge-Kutta method. In this method, we first obtain the equilibrium solution and the corresponding coefficients $c_{n_i, n_j}^{(p,q)}$, which define the initial state at $t = 0$. Then, the system is dynamically evolved using Eq. (6) to obtain $c_{n_i, n_j}^{(p,q)}(t)$. However, quantum fluctuations are needed to initiate and drive the quantum phase transition. To introduce the effects of quantum fluctuations, we add initial noise to the equilibrium coefficients $c_{n_i, n_j}^{(p,q)}$ of the state at the start of the quench. We first generate univariate random phases within the $[0, 2\pi]$ range and add them to the (phases of) nonzero coefficients. Next, we add density fluctuations by applying noise to the amplitudes of the coefficients. This is achieved by generating univariate random numbers within the $[0, \delta]$ range, where δ is set to be 10^{-4} in the present study. We consider ten randomized initial states to ensure reliable results using the previously described methods. Each initial state evolves in time by performing the appropriate parameter quench. We further calculate the physical observables of interest averaged over all these ten samples. Additionally, the observable is averaged across the entire lattice for each sample. To study the quench dynamics, we consider $N_{\text{lattice}} = 64 \times 64$.

B. Kibble-Zurek mechanism

In the present work, we consider a linear quench protocol given as

$$J(t) = J_i + \frac{(J_c - J_i)}{\tau_Q}(t + \tau_Q), \quad t \in [-\tau_Q, t], \quad (7)$$

which involves a quench time τ_Q to determine the quench rate. The critical value of J , denoted by J_c , is crossed at $t = 0$. It is assumed that the quench is initiated at time $t = -\tau_Q$, such that $J(-\tau_Q) = J_i$. The system's relaxation time determines the fate of the evolving state. The relaxation time is short

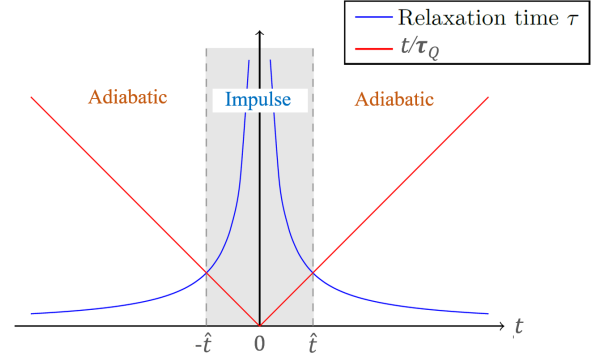


FIG. 3. The relaxation time (blue) and the inverse transition rate t/τ_Q (red) as a function of the t . The relaxation time equals the inverse transition rate at $-\hat{t}$ and \hat{t} . The shaded region between $-\hat{t}$ and \hat{t} is the impulse regime, where the system's relaxation time is larger than the timescale of the transition [42]. t is measured in units of \hbar/U .

when the quenched parameter is far from the critical point, resulting in an adiabatic evolution. However, as the critical point approaches, the divergence of relaxation time breaks the adiabaticity, leading to a frozen state. The time interval during which the state remains frozen is termed the impulse regime, followed by adiabatic evolution again from $t = \hat{t}$ (delayed time or transition time). Various regimes and timescales of the KZM are shown in Fig. 3. The nonadiabatic evolution of the system during the quench inevitably leads to excitations and defects in the evolved state.

In the Kibble-Zurek hypothesis, for a second-order phase transition, the scaling relation between τ_Q and \hat{t} is [42]

$$\hat{t} \propto \tau_Q^{\nu z / (1 + \nu z)}, \quad (8)$$

where ν is the critical exponent of the equilibrium correlation length ξ and z is the dynamical critical exponent associated with the relaxation time τ . Additionally, the scaling relation between the density of defects (N_d) and τ_Q in two dimensions is given by [42]

$$N_d(\hat{t}) \propto \tau_Q^{-2\nu / (1 + \nu z)}. \quad (9)$$

These relations predict the critical behavior of the system near the phase transition and the formation of topological defects during the nonadiabatic evolution of the system. In our case, i.e., during the transition from MI to the SF phase, the global U(1) symmetry spontaneously breaks and gives rise to the vortices. The density of vortices in an optical lattice system can be computed as [20–22,24]

$$N_v^\sigma = \sum_{p,q} |\Omega_{p,q}^\sigma|, \quad (10)$$

with

$$\Omega_{p,q}^\sigma = \frac{1}{4} [\sin(\theta_{p+1,q}^\sigma - \theta_{p,q}^\sigma) + \sin(\theta_{p+1,q+1}^\sigma - \theta_{p+1,q}^\sigma) - \sin(\theta_{p+1,q+1}^\sigma - \theta_{p,q+1}^\sigma) - \sin(\theta_{p,q+1}^\sigma - \theta_{p,q}^\sigma)]. \quad (11)$$

Here, $\theta_{p,q}^\sigma$ is the phase of the SF order parameter $\phi_{p,q}^\sigma$. The excess energy above the ground-state energy, termed as residual energy, is another quantity analogous to the defect

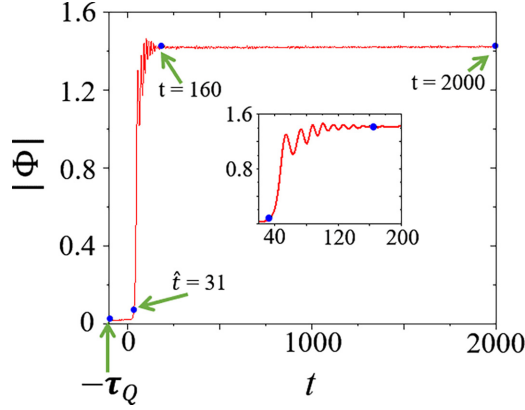


FIG. 4. The time evolution of $|\Phi|$ for the MI(2)-SF transition with $U_{\uparrow\downarrow} = 0.5$, $\mu = 1$, and $\tau_Q = 100$; quench is stopped at $t = \tau_Q$. $|\Phi|$ is nearly zero until adiabaticity is restored at \hat{t} . The stable $|\Phi|$ is marked at $t = 160$. In the inset, we show the enlarged view of the dynamical evolution at shorter times from $t = 20$ to $t = 200$. Unit of time is \hbar/U .

density [43–45]. This residual energy $E_{\text{res}}(\hat{t})$ is given by $E_{\text{res}}(\hat{t}) = E_{\text{fin}}(\hat{t}) - E_{\text{gs}}(\hat{t})$, where $E_{\text{fin}}(\hat{t}) = \langle \Psi(\hat{t}) | \hat{H}(\hat{t}) | \Psi(\hat{t}) \rangle$ denotes the energy of the system at time \hat{t} , while $E_{\text{gs}} = \langle \Psi_{\text{gs}} | \hat{H}(\hat{t}) | \Psi_{\text{gs}} \rangle$ is the ground-state energy for the Hamiltonian at time \hat{t} . The scaling relation for residual energy is $E_{\text{res}}(\hat{t}) \propto \tau_Q^{-2\nu/(1+\nu z)}$ [43–45]. The scaling relations are valid at \hat{t} , but it is not easy to estimate \hat{t} from numerical simulations. Prior works are based on determining \hat{t} based on Φ [20–23,25]. The growth time of the superfluid order parameter depends on the number of random fluctuations, as pointed out in Ref. [46]. We choose the protocol in Ref. [24] to determine \hat{t} . We calculate the overlap $O(t) = |\langle \Psi(0) | \Psi(t) \rangle|$. Since the dynamics are frozen in the impulse regime, $O(t)$ would be equal to unity in this regime; as soon as it deviates from unity, it indicates that the adiabatic regime has begun and that time instant is \hat{t} . The observables Φ , N_v^σ , E_{res} , and $O(t)$ relevant to quench dynamics are obtained by averaging over ten initial states perturbed by different random noise distributions.

IV. RESULTS AND DISCUSSIONS

A. $U_{\uparrow\downarrow} = 0.5$

1. MI(2) to SF phase transition

Starting from $J_i = 0.02$ deep within the MI lobe, we quench the hopping parameter to $J_f = 0.064$ within the SF phase for $\mu = 1$. We confirm the slowing down of transition from the growth of the superfluid order parameter that starts after the critical value J_c is passed at $t = 0$. We show one such dynamics for $\tau_Q = 100$ in Fig. 4. After $t = \hat{t} = 31$, $|\Phi|$ shows a sudden increase followed by rapid oscillations; at a longer time, the $|\Phi|$ stabilizes after small oscillatory transients. Due to the random noise added to the initial Gutzwiller coefficients, there are many vortices at the beginning of the quench. During the MI to SF phase transition, when the system enters the SF phase, one expects a coherent phase throughout the system. This is due to breaking of U(1) global gauge symmetry. However, the quench dynamics leads to the formation

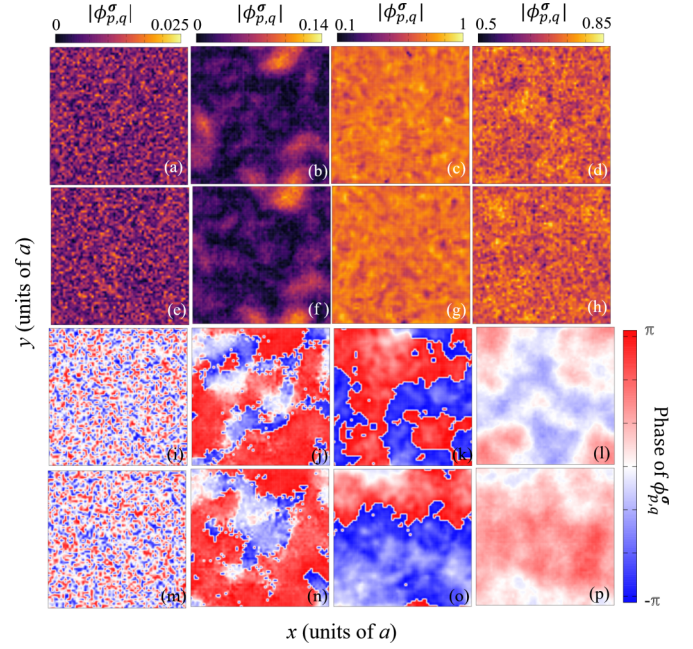


FIG. 5. $|\phi_{p,q}^\uparrow|$ at (a) $t = -100$, (b) $t = 31$, (c) $t = 160$, and (d) $t = 2000$ for MI(2)-SF phase transitions corresponding to the time evolution in Fig. 4. Similarly, $|\phi_{p,q}^\downarrow|$ at the same instants are in (e)–(h). Phases corresponding to $|\phi_{p,q}^\uparrow|$ in (a)–(d) are shown in (i)–(l), and the same for $|\phi_{p,q}^\downarrow|$ in (e)–(h) are in (m)–(p).

of domains in the system, indicating local choices of broken symmetry in the SF phase. This results in a domain structure as predicted by the KZM. The phase singularities at the domain boundaries correspond to the vortices, as confirmed by the phase variations. As the system enters the deep SF phase, the size of domains increases through domain merging. This results in decreased topological defects due to pair annihilation, and the system attains phase coherence at long-time evolution.

To illustrate the domain formation and merging in the quench dynamics starting with a single randomized initial state at $t = -\tau_Q = -100$, we presented the snapshots of $|\phi_{p,q}^\sigma(t)|$ and the respective phases in Fig. 5. At the beginning of the quench, the $\phi_{p,q}^\sigma$ have random lattice-site distributions with peak values of $|\phi_{p,q}^\sigma|$ nearly zero (see the first column of Fig. 5). At $t = \hat{t}$, $|\phi_{p,q}^\sigma|$ acquire relatively large peak values accompanied by domain formation (cf. the second column of Fig. 5). At $t = 160$, $|\phi_{p,q}^\sigma|$ acquire almost uniform distributions while their respective phases still have some phase singularities (see the third column of Fig. 5). After a very long time of evolution at $t = 2000$, the system relaxes into an almost uniform state where the component densities and phases are both quasi-uniform, as in the last column of Fig. 5.

To study the scaling laws, we consider a range of quench times from $\tau_Q = 30$ to $\tau_Q = 400$. We determine \hat{t} corresponding to each τ_Q following the overlap protocol. \hat{t} increases with an increase in τ_Q as is evident in Fig. 6(a). However, the residual energy E_{res} decreases with τ_Q [cf. Fig. 6(b)] as $J(\hat{t})$ approaches the critical tunneling strength J_c with an increasing τ_Q , (see Table I). Both observables follow power-law

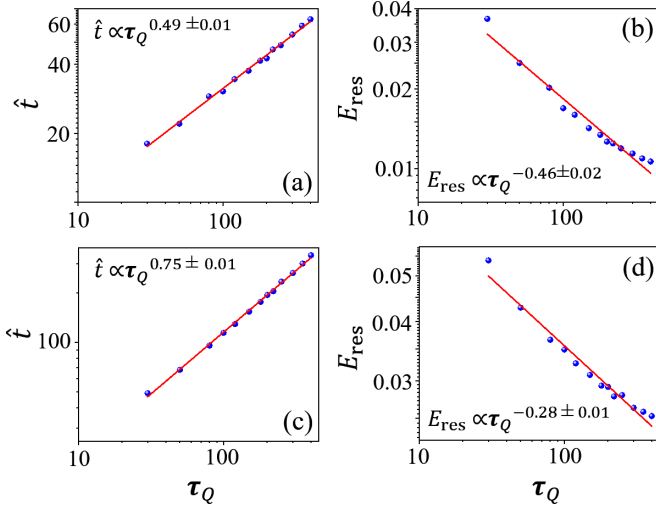


FIG. 6. For MI(2)-SF transition with $U_{\uparrow\downarrow} = 0.5$: (a) \hat{t} as a function of τ_Q on a log-log scale with the critical exponent of 0.49 ± 0.01 and (b) E_{res} as a function of τ_Q on the log-log scale with -0.46 ± 0.02 as the critical exponent. (c) and (d) are, similarly, the \hat{t} and E_{res} as functions of τ_Q on the log-log scale for MI(1)-SF transition with $U_{\uparrow\downarrow} = 0.5$. Unit of time is \hbar/U and E_{res} is in units of U .

scaling with the critical exponents $\nu = 0.45$ and $z = 2.13$. It is pertinent to note that the critical values obtained in our scaling analysis are in good agreement with the values predicted by the mean-field theory ($\nu = 0.5$ and $z = 2$) [5].

2. MI(1) to SF phase transition

The key difference between MI(2) and MI(1) of the TBHM is the density in-homogeneity, as shown in the equilibrium lattice-site distributions [see Figs. 1(e) to 1(h)]. This results in several differences in quench dynamics. One is that the impulse-regime size increases compared to the MI(2)-SF transition for each τ_Q . This is supported by the fact that, for the MI(2)-SF transition $J(\hat{t})$ always lies between J_c to $2J_c - J_i$, but here it is not the case. Fixing μ at 0.25, we quench J from $J_i = 0.01$ to a sufficiently high hopping strength $J_f = 0.0604$, so that $J(\hat{t})$ lies in between J_i and J_f . The critical value J_c of the MI(1)-SF transition is 0.0268. For smaller τ_Q up to about $\tau_Q = 150$, $J(\hat{t})$ is greater than $2J_c - J_i = 0.0436$. Even for the largest value of $\tau_Q = 400$ considered in the present study, $J(\hat{t})$ is 0.041 as reported in Table II. Another difference is that, due to the absence of particles of at least one species at each lattice site, the vortex density does not give a fair idea about the actual number of vortices. Due to the increase in transition time compared to the MI(2)-SF case, the exponent of transition time with τ_Q is higher, whereas the magnitude of the exponent of residual energy is lower. However, transition

TABLE I. The $J(\hat{t})$ for different τ_Q 's during quench dynamics from MI(2) to SF phase with $\mu = 1$ and $U_{\uparrow\downarrow} = 0.5$. The critical value of hopping strength $J_c = 0.042$.

τ_Q	30	50	80	100	150	200	300	400
$J(\hat{t})$	0.055	0.052	0.050	0.049	0.048	0.047	0.046	0.045

TABLE II. The $J(\hat{t})$ for different τ_Q 's during the quench dynamics from MI(1) to SF phase with $\mu = 0.25$ and $U_{\uparrow\downarrow} = 0.5$. The critical hopping strength is $J_c = 0.0268$.

τ_Q	30	50	80	100	150	200	300	400
$J(\hat{t})$	0.054	0.05	0.047	0.046	0.044	0.043	0.042	0.041

time and residual energy still follow power-law scaling with τ_Q as shown in Figs. 6(c) and 6(d).

We have shown the evolution of the superfluid order parameter for $\tau_Q = 100$ in Fig. 7; quench is stopped at $t = 130$ in this case. $|\Phi|$ is close to zero till $t = \hat{t} = 116$, after which it increases rapidly, followed by oscillations persisting over long periods during which it increases gradually. This starkly contrasts with the MI(2)-SF transition, where the order parameter stabilizes much sooner. To see how differently the state relaxes after the quench, we provide snapshots of the amplitude and corresponding phases of $\phi_{p,q}^\sigma$ at various time instants in Fig. 8. At the start of the quench at $t = -100$, $\phi_{p,q}^\sigma$ are randomized (see the first column of Fig. 8). Later, at $t = \hat{t} = 116$, a few superfluid domains have started to appear (cf. the second column of Fig. 8). The number of superfluid domains has increased and phases of the order parameters also exhibit domain formation in the third column at $t = 155$; this is when oscillations in $|\Phi|$ are triggered. Even after a long period of evolution at $t = 2000$, the $\phi_{p,q}^\sigma$ do not achieve homogeneous distributions, unlike for the MI(2)-SF transition.

B. $U_{\uparrow\downarrow} = 0.9$

We further discuss quench dynamics at higher interspecies interaction strength close to the immiscibility criterion but still in the miscible domain. From Fig. 1, the phase transition for $\mu = 1.33$ is a first-order MI(2)-SF transition. This, as mentioned earlier, is in contrast to the MI(2)-SF and MI(1)-SF transition for $U_{\uparrow\downarrow} = 0.5$. Although some traits of second-order MI(2)-SF transition, discussed in Sec. IV A 1 like slowing down of the transition, oscillations of $|\Phi|$ about a

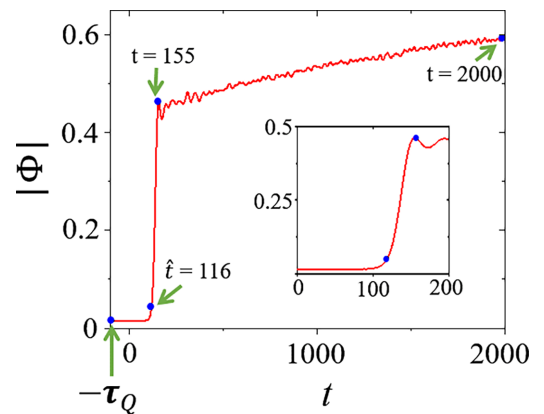


FIG. 7. $|\Phi|$ as a function of time t for MI(1)-SF transitions at $U_{\uparrow\downarrow} = 0.5$, $\mu = 0.25$, and $\tau_Q = 100$. $|\Phi|$ remains nearly zero for $t < \hat{t} = 116$. The hopping quench is performed until $t = 130$. The exponential increase in $|\Phi|$ followed by oscillations are shown in the inset with t varying from $t = 0$ to $t = 200$. Unit of time is \hbar/U .

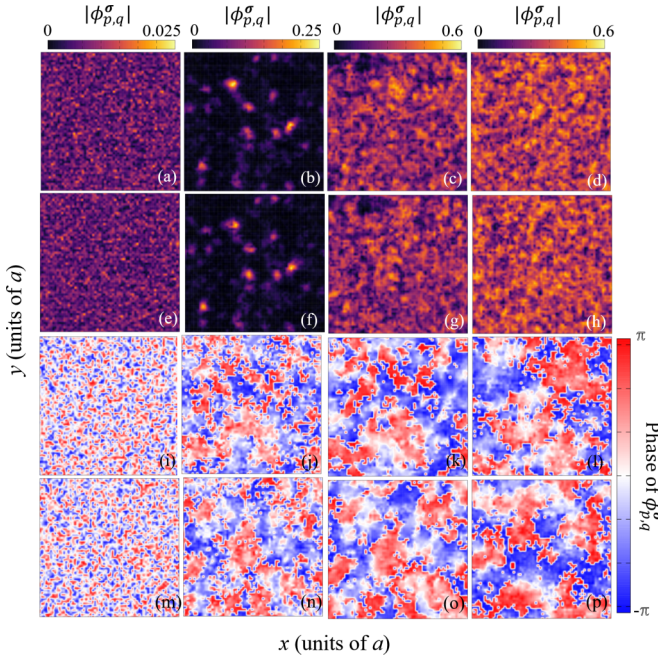


FIG. 8. $|\phi_{p,q}^\uparrow|$ at (a) $t = -100$, (b) $t = 116$, (c) $t = 155$, and (d) $t = 2000$ for MI(1)-SF phase transitions corresponding to the time evolution in Fig. 7. Similarly, $|\phi_{p,q}^\downarrow|$ at the same instants are in (e)–(h). Phases corresponding to $|\phi_{p,q}^\uparrow|$ in (a)–(d) are shown in (i)–(l), and the same for $|\phi_{p,q}^\downarrow|$ in (e)–(h) are in (m)–(p).

fixed value, order parameter relaxing into an almost complete uniform state after free evolution, and power-law scaling of \hat{t} and E_{res} with τ_Q are present, there is a striking difference in the exponents. The scaling for \hat{t} and $E_{\text{res}}(\hat{t})$ with respect to τ_Q with critical exponents of 0.36 ± 0.02 and -0.35 ± 0.02 , respectively, is shown in Fig. 9.

The quench dynamics and the exponents in the scaling laws of the second-order MI(1)-SF transition for $U_{\uparrow\downarrow} = 0.9$ remain almost similar to the MI(1)-SF transition for $U_{\uparrow\downarrow} = 0.5$ as discussed in Sec. IV A 2 and are not shown here for brevity.

C. $U_{\uparrow\downarrow} = 1.5$

Finally, we discuss quench dynamics for the phase-separated regime, where one of the two components occupies the lattice site. Starting from $\mu = 1.45$ and $J = 0$, correspond-

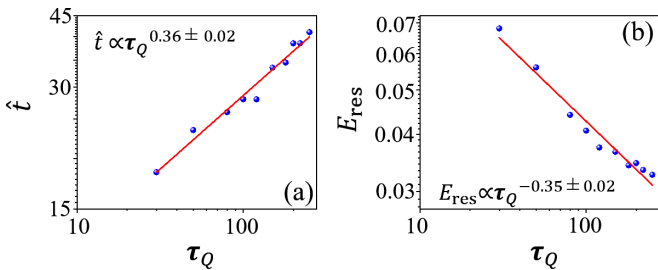


FIG. 9. For first-order MI(2)-SF phase transition at $U_{\uparrow\downarrow} = 0.9$ and $\mu = 1.33$: (a) \hat{t} as a function of τ_Q with the critical exponent of 0.36 ± 0.02 and (b) E_{res} as a function of τ_Q on log-log scale with -0.35 ± 0.02 as the critical exponent. Unit of time is \hbar/U and E_{res} is in units of U .

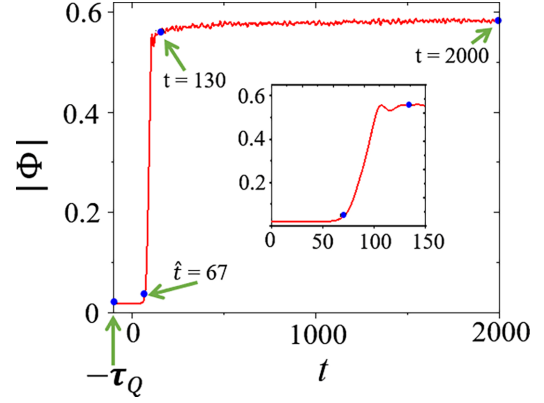


FIG. 10. The evolution of $|\Phi|$ with t for MI(2)-SF transitions at $U_{\uparrow\downarrow} = 1.5$, $\mu = 1.45$, and $\tau_Q = 100$. $|\Phi|$ is close to zero until $\hat{t} = 67$, followed by a rapid increase period. The exponential increase in $|\Phi|$ followed by oscillations are shown in the inset with t varying from $t = 0$ to $t = 150$. Unit of time is \hbar/U .

ing to the MI(2) lobe, we perform a quench that terminates at $J = 0.0516$, lying well within the SF phase. The transition is indicated by the growth of the superfluid order parameter at $t = \hat{t}$ and occurs after crossing the critical $J_c = 0.0258$, as demonstrated in Fig. 10 for $\tau_Q = 100$. The J quench is terminated at $t = \tau_Q$, but the system is freely evolved up to $t = 2000$ with the tunneling strength fixed at $J(\tau_Q)$. Figure 11 provides snapshots of $|\phi_{p,q}^\sigma|$ and the corresponding phase of $\phi_{p,q}^\sigma$ at different times. Domain formation begins at $t = \hat{t} = 67$, and at a later time $t = 130$, $|\phi_{p,q}^\sigma|$ have acquired many domains with respective phases exhibiting domain merging (cf.

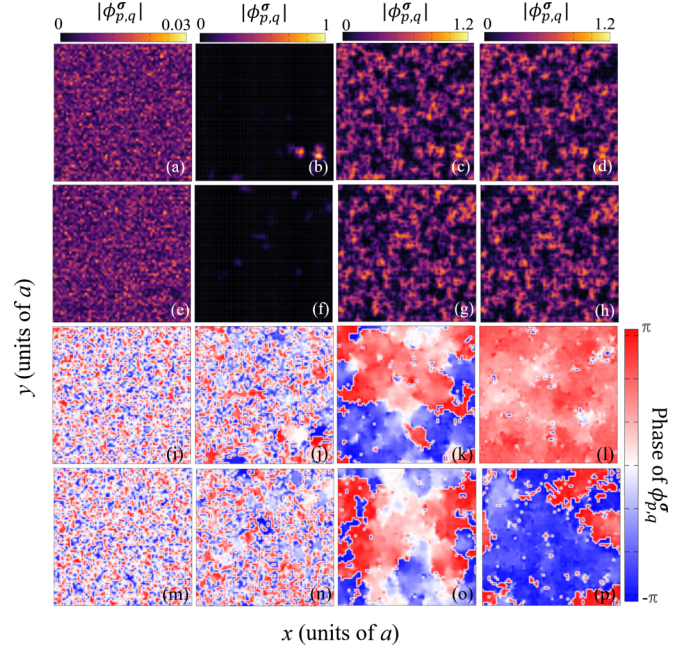


FIG. 11. $|\phi_{p,q}^\uparrow|$ at (a) $t = -100$, (b) $t = 67$, (c) $t = 130$, and (d) $t = 2000$ for MI(2)-SF phase transitions corresponding to the time evolution in Fig. 10. Similarly, $|\phi_{p,q}^\downarrow|$ at the same instants are in (e)–(h). Phases corresponding to $|\phi_{p,q}^\uparrow|$ in (a)–(d) are shown in (i)–(l), and the same for $|\phi_{p,q}^\downarrow|$ in (e)–(h) are in (m)–(p).

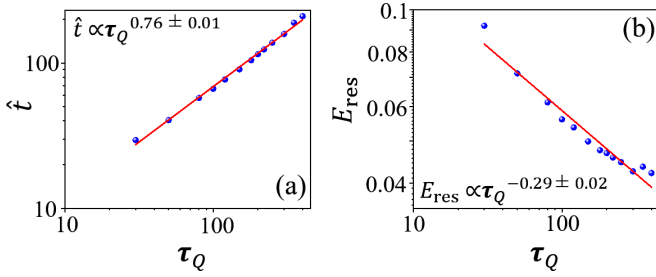


FIG. 12. For MI(2)-SF phase transition at $U_{\uparrow\downarrow} = 1.5$: (a) \hat{t} as a function of τ_Q with the critical exponent of 0.76 ± 0.01 and (b) E_{res} as a function of τ_Q on log-log scale with -0.29 ± 0.01 as the critical exponents. The critical exponents are similar to those displayed in Figs. 6(c) and 6(d). Unit of time is \hbar/U and E_{res} is in units of U .

the second and the third columns of Fig. 11). The component order parameters at $t = 2000$ show no discernible difference from those at $t = 130$ (see the last column of Fig. 11). The late time evolution as seen in these figures, especially of phases, is indicative of the phase ordering.

Similarly, the dynamics at the other two $U_{\uparrow\downarrow}$ values discussed previously, \hat{t} and E_{res} , follow power-law scaling as shown in Figs. 12(a) and 12(b) and with the critical exponents similar to those for the MI(1)-SF transition in the miscible domain. This is evident from Figs. 6(c) and 6(d) and Figs. 12(a) and 12(b). Since the system is in the immiscible phase, both MI(1) and MI(2) have inhomogeneous atomic occupancy distributions $\rho_{p,q}^\sigma$. This may be the reason that the quench dynamics of MI(1)-SF for $U_{\uparrow\downarrow} = 1.5$ (not presented here) is similar to that of the MI(2)-SF transition.

V. CONCLUSION

We studied the out-of-equilibrium dynamics of the two-component Bose-Hubbard model when the tunneling strength J is quenched across the MI-SF criticality. The equilibrium phase diagram and related phase transitions depend on interspecies interaction strength. We observed that the average filling of the MI lobes and the order of the phase transitions lead to different dynamics from what was observed in a single-component BHM. The MI-SF phase transitions, in the miscible regime, from the Mott lobes with an average

occupancy of 1 or 2 are second-order for $U_{\uparrow\downarrow}$ less than a critical strength above which the transitions at and around the tip of the MI(2) lobe are first order. The critical exponents of the second-order phase transition from homogeneous MI to superfluid phase, calculated using scaling analysis, are in good agreement with the mean-field predictions. Due to the inhomogeneity of the atomic occupancy in MI(1), the impulse regime is extended across the MI(1)-SF phase transition at $U_{\uparrow\downarrow} = 0.5$. In the immiscible regime, the power-law scaling of the exponents is maintained with exponents similar to those for the MI(1)-SF phase transition in the miscible regime. Although the KZM is unsuitable for the first-order quantum phase transition, defining scaling relations is possible. However, the nature of the dynamical evolution is very different. The use of beyond mean-field methods such as the projection-operator method [47] is expected to yield qualitatively similar quench dynamics of the order parameter, as discussed in the present work. Furthermore, the cluster Guzwiller mean-field approach, which enhances the intersite atomic correlations, may advance the critical exponents towards the equilibrium values [48]. We hope the phenomena discussed in the present work can be realized in cold-atom experiments on strongly correlated bosonic mixtures in optical lattices. The exploration in this direction may unveil the role of coupling in quantum mixtures and the applicability of the Kibble-Zurek mechanism to two-component Bose-Hubbard models. The presence of synthetic spin-orbit coupling in Bose-Bose mixtures leads to novel finite-momentum superfluids [34,49,50]. Thus, the investigations of the quench dynamics and criticality of spin-orbit-coupled mixtures in optical lattices could be a natural extension of the present work.

ACKNOWLEDGMENTS

We thank Deepak Gaur and Hrushikesh Sable for their valuable discussions. K.S. acknowledges the support from IAMS, Academia Sinica, Taiwan. K.S., D.A., and S.G. acknowledge support from the Science and Engineering Research Board, Department of Science and Technology, Government of India through Projects No. SRG/2023/001569, No. CRG/2022/007099, and No. CRG/2021/002597, respectively.

-
- [1] I. Bloch, J. Dalibard, and S. Nascimbène, *Nat. Phys.* **8**, 267 (2012).
- [2] M. Lewenstein, A. Sanpera, V. Ahufinger, B. Damski, A. Sen(De) and U. S. Lewenstein, *Adv. Phys.* **56**, 243 (2007).
- [3] D. Jaksch, C. Bruder, J. I. Cirac, C. W. Gardiner, and P. Zoller, *Phys. Rev. Lett.* **81**, 3108 (1998).
- [4] M. Greiner, O. Mandel, T. Esslinger, T. W. Hänsch and I. Bloch, *Nature (London)* **415**, 39 (2002).
- [5] M. P. A. Fisher, P. B. Weichman, G. Grinstein, and D. S. Fisher, *Phys. Rev. B* **40**, 546 (1989).
- [6] S. Sachdev, *Quantum Phase Transitions* (Cambridge University Press, Cambridge, England, 2001).
- [7] D. Jaksch, H. J. Briegel, J. I. Cirac, C. W. Gardiner, and P. Zoller, *Phys. Rev. Lett.* **82**, 1975 (1999); G. K. Brennen, C. M. Caves, P. S. Jessen, and I. H. Deutsch, **82**, 1060 (1999).
- [8] E. Farhi, J. Goldstone, S. Gutmann, J. Lapan, A. Lundgren, and D. Preda, *Science* **292**, 472 (2001).
- [9] T. W. B. Kibble, *J. Phys. A* **9**, 1387 (1976).
- [10] W. H. Zurek, *Nature (London)* **317**, 505 (1985).
- [11] T. W. B. Kibble, *Phys. Rep.* **67**, 183 (1980).
- [12] W. H. Zurek, *Acta Phys. Pol. B* **24**, 1301 (1993); *Phys. Rep.* **276**, 177 (1996).
- [13] N. Bevis, M. Hindmarsh, M. Kunz, and J. Urrestilla, *Phys. Rev. Lett.* **100**, 021301 (2008).

- [14] V. M. H. Ruutu, V. B. Eltsov, A. J. Gill, T. W. B. Kibble, M. Krusius, Y. G. Makhlin, B. Plaçais, G. E. Volovik, and W. Xu, *Nature (London)* **382**, 334 (1996).
- [15] R. Carmi, E. Polturak, and G. Koren, *Phys. Rev. Lett.* **84**, 4966 (2000).
- [16] I. Chuang, R. Durrer, N. Turok, and B. Yurke, *Science* **251**, 1336 (1991).
- [17] L. E. Sadler, J. M. Higbie, S. R. Leslie, M. Vengalattore, and D. M. Stamper-Kurn, *Nature (London)* **443**, 312 (2006); T. Donner, S. Ritter, T. Bourdel, A. Ottl, M. Kohl, and T. Esslinger, *Science* **315**, 1556 (2007); C. N. Weiler, T. W. Neely, D. R. Scherer, A. S. Bradley, M. J. Davis, and B. P. Anderson, *Nature (London)* **455**, 948 (2008); G. Lamporesi, S. Donadello, S. Serafini, F. Dalfovo, and G. Ferrari, *Nat. Phys.* **9**, 656 (2013); E. Nicklas, M. Karl, M. Höfer, A. Johnson, W. Muessel, H. Strobel, J. Tomković, T. Gasenzer, and M. K. Oberthaler, *Phys. Rev. Lett.* **115**, 245301 (2015); N. Navon, A. L. Gaunt, R. P. Smith, and Z. Hadzibabic, *Science* **347**, 167 (2015); M. Anquez, B. A. Robbins, H. M. Bharath, M. Boguslawski, T. M. Hoang, and M. S. Chapman, *Phys. Rev. Lett.* **116**, 155301 (2016); A. Keesling, A. Omran, H. Levine, H. Bernien, H. Pichler, S. Choi, R. Samajdar, S. Schwartz, P. Silvi, S. Sachdev, P. Zoller, M. Endres, M. Greiner, V. Vuletić, and M. D. Lukin, *Nature (London)* **568**, 207 (2019); C.-R. Yi, S. Liu, R.-H. Jiao, J.-Y. Zhang, Y.-S. Zhang, and S. Chen, *Phys. Rev. Lett.* **125**, 260603 (2020).
- [18] D. Chen, M. White, C. Borries, and B. DeMarco, *Phys. Rev. Lett.* **106**, 235304 (2011); L. W. Clark, L. Feng, and C. Chin, *Science* **354**, 606 (2016).
- [19] B. Ko, J. W. Park, and Y. Shin, *Nat. Phys.* **15**, 1227 (2019); X.-P. Liu, X.-C. Yao, Y. Deng, Y.-X. Wang, X.-Q. Wang, X. Li, Q. Chen, Y.-A. Chen, and J.-W. Pan, *Phys. Rev. Res.* **3**, 043115 (2021).
- [20] K. Shimizu, Y. Kuno, T. Hirano, and I. Ichinose, *Phys. Rev. A* **97**, 033626 (2018).
- [21] K. Shimizu, T. Hirano, J. Park, Y. Kuno, and I. Ichinose, *Phys. Rev. A* **98**, 063603 (2018).
- [22] Y. Zhou, Y. Li, R. Nath, and W. Li, *Phys. Rev. A* **101**, 013427 (2020).
- [23] K. Shimizu, T. Hirano, J. Park, Y. Kuno, and I. Ichinose, *New J. Phys.* **20**, 083006 (2018).
- [24] H. Sable, D. Gaur, S. Bandyopadhyay, R. Nath, and D. Angom, *arXiv:2106.01725*.
- [25] H. Wang, X. He, S. Li, H. Li, and B. Liu, *arXiv:2209.12408*.
- [26] S. Braun, M. Friesdorf, S. S. Hodgman, M. Schreiber, J. P. Ronzheimer, A. Riera, M. d. Rey, I. Bloch, J. Eisert, and U. Schneider, *Proc. Natl. Acad. Sci.* **112**, 3641 (2015).
- [27] J.-M. Cui, Y.-F. Huang, Z. Wang, D.-Y. Cao, J. Wang, W.-M. Lv, L. Luo, A. d. Campo, Y. Han, C.-F. Li, and G.-C. Guo, *Sci. Rep.* **6**, 33381 (2016).
- [28] E. Demler and F. Zhou, *Phys. Rev. Lett.* **88**, 163001 (2002); B. Paredes and J. I. Cirac, *ibid.* **90**, 150402 (2003); A. B. Kuklov and B. V. Svistunov, *ibid.* **90**, 100401 (2003); S. K. Yip, *ibid.* **90**, 250402 (2003).
- [29] Y. Kato, D. Yamamoto, and I. Danshita, *Phys. Rev. Lett.* **112**, 055301 (2014).
- [30] L.-Y. Qiu, H.-Y. Liang, Y.-B. Yang, H.-X. Yang, T. Tian, Y. Xu, and L.-M. Duan, *Sci. Adv.* **6**, eaba7292 (2020).
- [31] H.-Y. Liang, L.-Y. Qiu, Y.-B. Yang, H.-X. Yang, T. Tian, Y. Xu, and L.-M. Duan, *New J. Phys.* **23**, 033038 (2021).
- [32] B. Damski, L. Santos, E. Tiemann, M. Lewenstein, S. Kotochigova, P. Julienne, and P. Zoller, *Phys. Rev. Lett.* **90**, 110401 (2003).
- [33] D. S. Rokhsar and B. G. Kotliar, *Phys. Rev. B* **44**, 10328 (1991); W. Krauth, M. Caffarel, and J.-P. Bouchaud, **45**, 3137 (1992); K. Sheshadri, H. R. Krishnamurthy, R. Pandit, and T. V. Ramakrishnan, *Europhys. Lett.* **22**, 257 (1993); R. Bai, S. Bandyopadhyay, S. Pal, K. Suthar, and D. Angom, *Phys. Rev. A* **98**, 023606 (2018).
- [34] K. Suthar, P. Kaur, S. Gautam, and D. Angom, *Phys. Rev. A* **104**, 043320 (2021).
- [35] S. Anufriev and T. A. Zaleski, *Phys. Rev. A* **94**, 043613 (2016).
- [36] R. Bai, D. Gaur, H. Sable, S. Bandyopadhyay, K. Suthar, and D. Angom, *Phys. Rev. A* **102**, 043309 (2020).
- [37] T. Ozaki, I. Danshita, and T. Nikuni, *arXiv:1210.1370*.
- [38] D. Yamamoto, T. Ozaki, C. A. R. Sá de Melo, and I. Danshita, *Phys. Rev. A* **88**, 033624 (2013).
- [39] L. de Forges de Parny, F. Hébert, V. G. Rousseau, R. T. Scalettar, and G. G. Batrouni, *Phys. Rev. B* **84**, 064529 (2011).
- [40] D. van Oosten, P. van der Straten, and H. T. C. Stoof, *Phys. Rev. A* **63**, 053601 (2001).
- [41] K. Mitra, C. J. Williams, and C. A. R. Sá de Melo, *Phys. Rev. A* **77**, 033607 (2008).
- [42] A. del Campo and W. H. Zurek, *Int. J. Mod. Phys. A* **29**, 1430018 (2014).
- [43] A. Dhar, D. Rossini, and B. P. Das, *Phys. Rev. A* **92**, 033610 (2015).
- [44] T. Caneva, R. Fazio, and G. E. Santoro, *Phys. Rev. B* **78**, 104426 (2008).
- [45] F. Pellegrini, S. Montangero, G. E. Santoro, and R. Fazio, *Phys. Rev. B* **77**, 140404(R) (2008).
- [46] Y. Machida and K. Kasamatsu, *Phys. Rev. A* **103**, 013310 (2021).
- [47] C. Trefzger and K. Sengupta, *Phys. Rev. Lett.* **106**, 095702 (2011); A. Dutta, C. Trefzger, and K. Sengupta, *Phys. Rev. B* **86**, 085140 (2012).
- [48] D. Gaur, H. Sable, and D. Angom, *arXiv:2309.06272*.
- [49] M. Yan, Y. Qian, H.-Y. Hui, M. Gong, C. Zhang, and V. W. Scarola, *Phys. Rev. A* **96**, 053619 (2017).
- [50] S. Mandal, K. Saha, and K. Sengupta, *Phys. Rev. B* **86**, 155101 (2012).